



An Accurate Transient Analysis of High-Speed Package Interconnects Using Convolution Technique

WENDEMAGEGNEHU T. BEYENE AND CHUCK YUAN

Rambus Inc., Los Altos, CA 94022, USA
E-mail: wbeyene@rambus.com; xyuan@rambus.com

Abstract. An accurate transient analysis of a package interconnect requires the modeling and analysis of conductor and dielectric losses, as well as other high-frequency effects of 3D structures. The skin effect and dispersion of interconnects are more accurately modeled in frequency domain. Consequently, an accurate time-domain simulation of such a system is only possible using convolution techniques. Although the convolution method is well understood, the application of windowing for frequency-dependent interconnect analysis is less so. In this paper, we present the practical considerations of window selection and its application to improve the accuracy of convolution simulators. We introduce the Tukey window and study the tradeoff between how smoothly data can be set to zero to avoid aliasing and suppress ripples and how much information tapering will discount at the edge of the window in order to obtain meaningful results. The bandlimiting effects of the Tukey window and other well-known windows are also compared. Finally, to verify the validity and accuracy of the proposed method, a wirebond PBGA package and a PCB-connector system are analyzed using the scattering parameters obtained from simulation and measurement, respectively.

Key Words: bandlimiting filter, convolution technique, plastic ball-grid-array (PBGA) package, Tukey window

I. Introduction

With the rapid advance of silicon process technology, it is now possible to design I/O circuits that operate at multi-gigabit data rates. Consequently, current digital applications are quickly moving to the gigabit data rate range in order to meet the high-bandwidth requirements of today's computing systems. For example, Rambus' *Yellowstone* signaling technology utilizes bi-directional low-swing Differential Rambus Signaling Level (*DRSL*) with a data transfer rate starting at 3.2 Gbps/pair and scalable to 6.4 Gbps/pair [1]. The high operating frequencies of such systems place increasing demands on the package and PCB interconnects. Therefore, accurate analysis of the interconnect systems over a wide frequency range is essential to optimize the performance of the overall system.

The packaging and interconnect design, modeling and simulation methodologies that are necessary to achieve these high data rates with conventional low-cost PCBs and packages are challenging [2]. In partic-

ular, the modeling and analysis of conductor and dielectric losses, as well as the other higher-frequency effects of connectors, plating stubs, line bends, crossovers, vias, solderballs, and wirebonds are complicated and require meticulous time- and frequency-domain simulation techniques. For example, frequency-dependent characteristics of interconnects such as skin effect and dispersion are more accurately modeled in the frequency domain. However, determining timing and voltage margins requires a time-domain simulation of the interconnects with nonlinear drivers and terminations. Conventional circuit simulation programs such as *SPICE* use circuit theory parameters and closed-form formulas or compact expressions to approximate the behaviors of interconnects in the time domain.

In order to simulate using *SPICE*, an interconnect typically is modeled by cascading a large number of lumped components including resistors, inductors and capacitors. For example, a signal net in a wirebond PBGA package is decomposed into many small sub-sections such as wirebonds, vias, solderballs, and

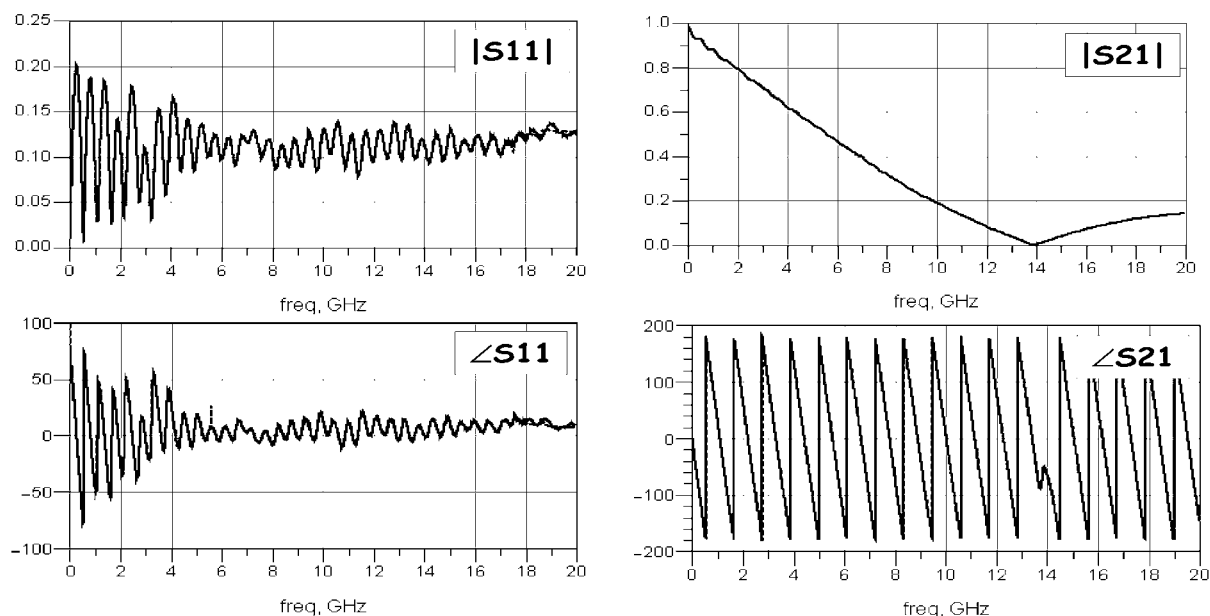


Fig. 1. The measured (solid line) and approximated (dashed line) magnitude and phase of reflection and transfer coefficients of a 6-in. coupled microstrips.

signal traces, each represented by passive circuit elements whose parameters are calculated using 2D electromagnetic field solvers. Although this approach is computationally inexpensive, it becomes less accurate at higher frequencies because it ignores the fringe effects and assumes pure TEM modes even for 3D transitions. In order to capture the interconnect's exact behavior over a wide frequency range, the number of circuit elements can significantly increase. For

example to capture the frequency-domain characteristics of 6-in. coupled microstrip lines on an FR4 PC board, over 5500 circuit elements are needed to accurately approximate the scattering parameters over 20 GHz as shown in Fig. 1. Even though the frequency-domain behavior of the system is captured quite well using higher-order networks, the time-domain responses oscillate and show ringing as shown in Fig. 2 due to the large number of circuit elements and nodes in

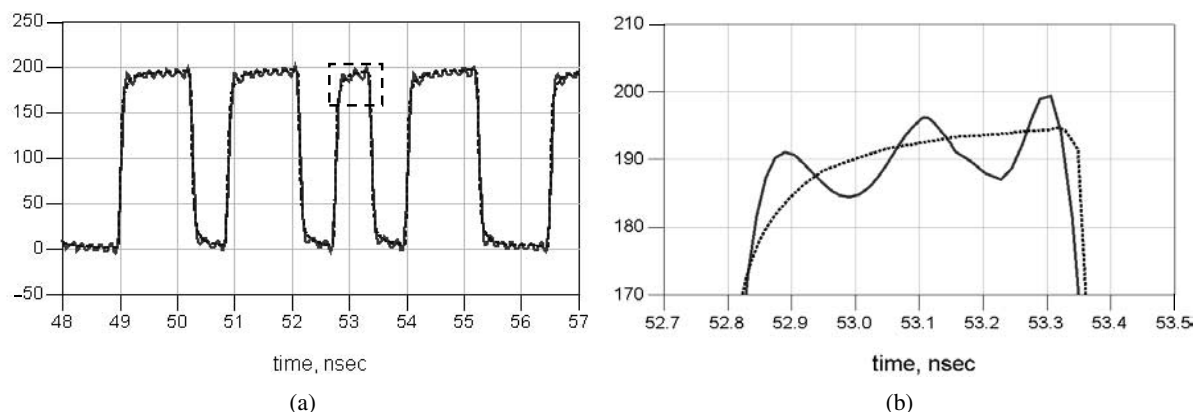


Fig. 2. The responses of a 6-in. coupled microstrip lines using measured data (dashed line) and approximated (solid line) using over 5500 circuit elements. (a) The output waveforms, (b) Magnified output waveforms.

the system. Consequently, this could create significant error and divergence in calculating the response and increase the simulation time by several orders of magnitude.

Recent models of lossy and dispersive transmission lines use more complex and sophisticated functional approximations in the frequency domain. Although these models often closely approximate the behavior of the devices, they fail to capture the true behavior under extreme cases [3]. Consequently, the time-domain results can deviate significantly from the correct waveforms when fast signals are present. Most of the compact models are noncausal. Therefore, simulation results generate incorrect delay and phase. For example, commercial circuit simulators that are based on these approximations give inconsistent time-domain responses when used to simulate identical networks of a simple cascade of two or more non-ideal transmission lines of fixed total length. Other commercial circuit and system simulation tools indirectly handle components defined by tabulated frequency-domain parameters using rational functions. This approximation is incorporated into the system after the sampled values are interpolated using rational functions. This intermediate approximation is essential due to the inherent limitations of the adopted simulation technique [4]. The robustness of this approach has yet to be verified for general applications.

One approach to accurately simulate transmission line systems is based on the convolution method [5–7]. This method requires numerical transforms of the frequency-domain data to time domain. The impulse responses of the transmission line system are used to solve the nonlinear convolution equations governing the line system and nonlinear driver and termination networks. The application of low-pass filtering to band-limit the frequency-domain data is often required in order to avoid impulse responses of infinite duration, Gibbs phenomena and aliasing errors that can accumulate and lead to convergence and numerical stability problems. As shown in Fig. 3, this method allows the use of frequency-domain parameters directly in simulation, thus minimizing the error introduced when converting the scattering parameters to more familiar network parameters to develop circuit representations. Therefore, the method avoids trial and error and optimization to extract model parameters.

This paper addresses the practical considerations of window selection and its application to reduce these undesired effects in convolution-based simulators. The

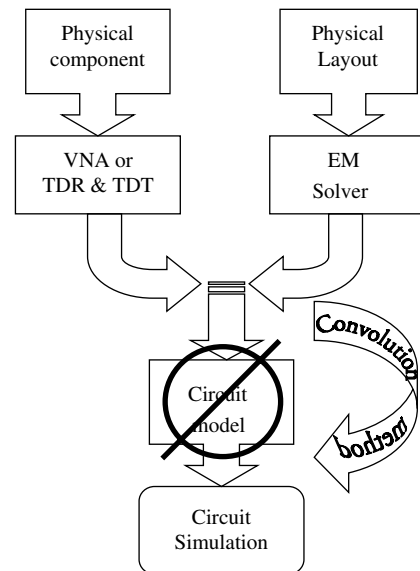


Fig. 3. Convolution-based simulation methodology of interconnects.

Tukey window is introduced for the first time for such applications. The major parameters that control the compromise between how smoothly the data can be set to zero to avoid aliasing and suppress ripples and the amount of information tapering discount at the edge of the window necessary to obtain meaningful results is addressed. Finally, the use of Tukey window to accurately analyze PBGA packages and PCB interconnect systems, in both time and frequency domains, is demonstrated. The effects of plating stubs, wirebonds, connectors, and other 3D structure are studied.

II. Windowing

Transient analysis of interconnects characterized by frequency-domain parameters, defined as functions of frequency or obtained as sample data from measurements or full-wave electromagnetic solvers can be problematic. The most straightforward approach is to calculate the impulse response of the network using the *IFFT* and applying the discrete time solution to solve the whole system for a given input waveform. Such an approach requires the impulse response be convolved with the entire computed input waveform at every simulation time step. The *IFFT* used to transform frequency-domain parameters into time-domain

data requires special attention to avoid aliasing and unwanted ringing that decreases the accuracy and efficiency of the simulation results.

The frequency-domain parameters do not always vanish at the high frequencies. For example, coupling parameters tend to asymmetrically approach non-zero constants as frequency increases. If these parameters are simply truncated, discontinuities are introduced at the boundaries, and the time-domain transforms of the parameters show ringing. Consequently, the output waveforms of a system characterized by such discontinuous parameters show significant ripples. This is because truncating the parameters abruptly in frequency domain is equivalent to using a rectangular window that has unity gain in the frequency range and zero outside. The transform of the rectangular window in time domain is a *sinc* function, which has a primary peak, and multiple secondary peaks that are slowly decaying.

One option to reduce the time-domain ripple associated with taking the *IFFT* is to multiply the frequency-domain data by a window that produces less ripple prior to transformation. Windows or low-pass filters are extensively used in many applications to smooth, interpolate, and denoise sampled data. In order to remove the effects of aliasing and undesired ringing of long duration, windows that have shapes smoother than the rectangular window can be used. An ideal window for our application is one that attempts to smoothly set the data to zero at the boundaries while not significantly distorting the data inside the window. The bandlimited spectrum is the product of the actual unbounded data and the window. Therefore, the impulse response of the interconnect is the convolution of the impulse response of the original or actual data and the transform of the window.

Some of the common window shapes often used as low-pass filters, Hamming, Gaussian, Blackman, Blackman-Harris, and Kaiser-Bessel, are shown in Fig. 4. Some of the figures of merit of these windows are also summarized in Table 1. The Kaiser-Bessel window has a parameter, window constant α , that modifies the transition width and stopband attenuation. The Blackman-Harris and Kaiser-Bessel windows show good amplitude resolution corresponding to low side-lobes in their transforms. This means that more of the energy is in the main lobe and less is in the ripple. If there is less energy in the ripple then the time-domain response also has smaller ripples and therefore a better function for windowing data. A detailed descrip-

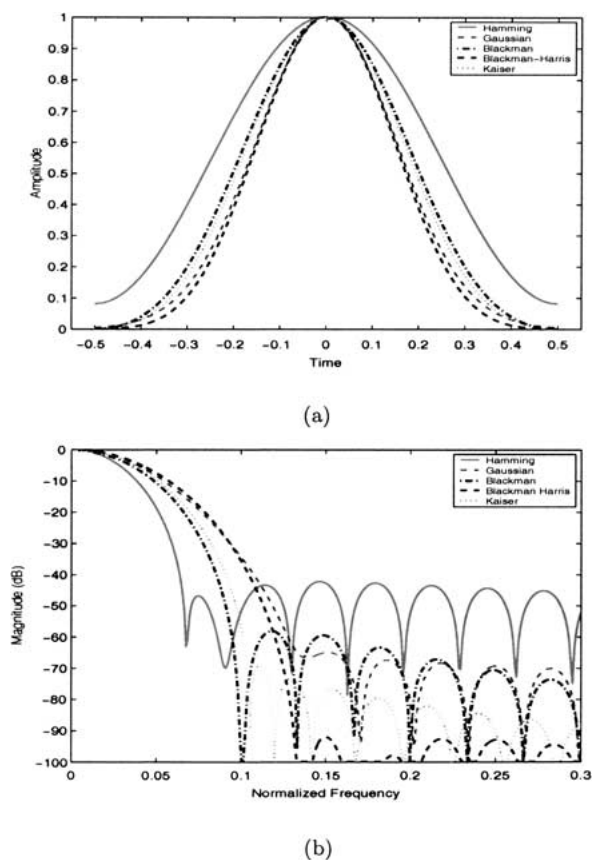


Fig. 4. Common windows. (a) Shape of the windows, (b) Log magnitude of transforms.

tion of the effects of various windows when used with discrete Fourier transforms can be found in [8]. The subsequent correction and extension are also found in [9].

Table 1. Windows and figures of merit.

Window Types	Peak Sidelobe (dB)	Asymptotic Decay (dB/octave)
Blackman	-58	-18
Blackman-Harris	-92	-6
Gaussian	-55	-6
Hamming	-31	-6
Hanning	-43	-18
Kaiser-Bessel ($\alpha = 3.5\pi$)	-82	-6
Rectangular	-13	-6
Tukey ($\alpha = 0.25$)	-14	-18
Tukey ($\alpha = 0.50$)	-15	-18
Tukey ($\alpha = 0.75$)	-19	-18

As shown in Section IV, while applying these windows smooths the spectrum, avoids aliasing and suppresses the ripples, it unfortunately causes the spectrum to be biased as the tapering modifies the parameters at the edge of the window. Since frequency-domain data can often be short, this severely limits the useful frequency range. Ideally, we want a window whose transform domain has as few ripples as possible while still maintaining as rectangular a shape as possible. However, choosing a good window involves trading off frequency and amplitude resolutions. A low-pass filter that provides a parameter to control this trade-off between how fast and how smooth the data can be set to zero is the Tukey window [8]. The Tukey window is defined as

$$w(n) = \begin{cases} 1 & \text{if } 0 \leq n \leq \alpha \frac{N}{2} \\ 0.5 + 0.5 \cos \left(\pi \frac{n - \alpha \frac{N}{2}}{2(1 - \alpha) \frac{N}{2}} \right) & \text{if } \alpha \frac{N}{2} \leq n \leq \frac{N}{2} \end{cases} \quad (1)$$

where $0 \leq \alpha \leq 1$, and n and N are the sample point and the total number of samples, respectively. This parameter modifies the transition width from passband to stopband. The Tukey windows for values of α equal to 0.25, 0.5, and 0.75 are shown in Fig. 5. The Tukey window is a product of a cos lobe window of width $\alpha \frac{N}{2}$ and a rectangle window of width $(1 - \alpha) \frac{N}{2}$. The rectangular and Hanning windows show the largest and smallest sidelobes of about -13 dB and -43 dB, respectively. Therefore, rectangular and Hanning windows have the largest and the smallest ripples, respectively, in the time-domain waveforms compared to the rest of the windows. The family of Tukey windows exhibits a range of sidelobe levels between the levels of the Hanning and rectangular windows. When α goes to 1, the Tukey window becomes a flat-topped window that quickly falls to zero near the edge of the interval resulting in the narrowest main lobes. Therefore, it gives the best frequency resolution as a rectangular window but introduces a significant ripple in the transform. When α goes to 0, the Tukey window approaches the Hanning window and its transform has lower sidelobes. There are two important properties of Tukey window that are relevant to our application. First, the Tukey window has a parameter to easily control where the tapering for the frequency-domain

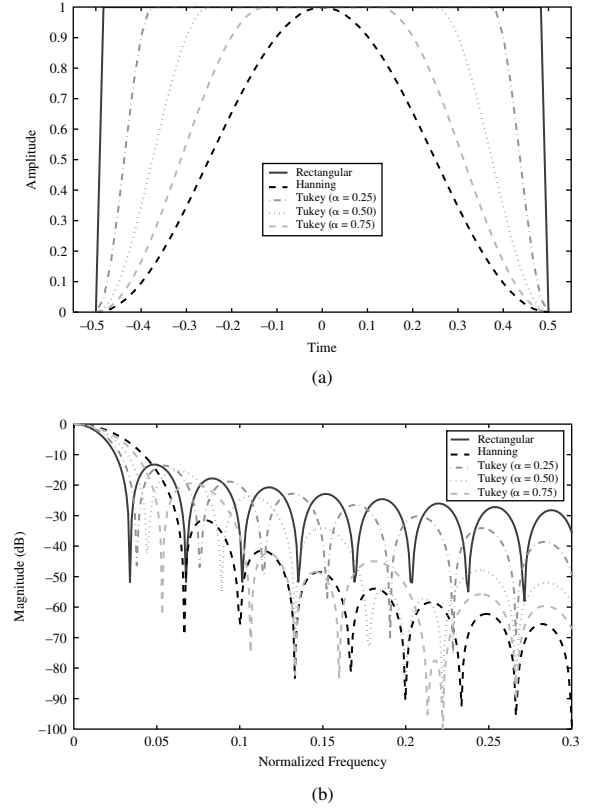


Fig. 5. Rectangular, Hanning, and 25%, 50%, 75% cosine taper (Tukey) windows. (a) Shape of the windows, (b) Log magnitude of transforms.

parameter starts, allowing preservation of the frequency-domain information. It evolves from a rectangular to a Hanning window as α decreases from 1 to 0. Secondly, the window function and its derivative are continuous, thus the transform decays as $(1/t^3)$ for large values of the transform variable, t . Thus the sidelobes decay -18 dB/octave causing the ripples in time-domain to die out quickly. The window can also be used to extrapolate data beyond the frequency range of the original data.

III. Scattering Parameter Formulation

Lumped circuit elements do not accurately represent package interconnects at higher frequencies. The accurate extraction of parameters of lossy transmission lines is very complex and most sophisticated transmission line models are not reliable over wide frequency ranges.

However, a scattering matrix exists for every linear, passive, and time-invariant network and is readily available from high-frequency measurements. They are suitable at high frequencies where traveling wave concepts predominate over lumped element techniques. The N-port scattering parameters of complex interconnect structures can be obtained from frequency-domain measurements with high accuracy by using one of the commercially available network analyzers. They can be accurately measured over a wider frequency range using careful calibration techniques. Time-domain impulse responses can also be obtained from reflection and transmission measurements using a high-speed oscilloscope with *TDR* and *TDT* options. The frequency-domain scattering matrix relates incident to reflected waves as

$$\mathbf{B}(\omega) = \mathbf{S}(\omega)\mathbf{A}(\omega) \quad (2)$$

where $\mathbf{S}(\omega)$ is the scattering matrix describing the system, and $\mathbf{A}(\omega)$ and $\mathbf{B}(\omega)$ are the forward and backward traveling wave vectors, respectively, in the frequency domain. The main diagonal entries of $\mathbf{S}(\omega)$ are reflection coefficients and those along the off diagonal are transmission coefficients. In order to be able to handle the nonlinear devices, the time-domain formulation can be obtained by applying IFFT on (2) resulting with the convolution given as

$$\mathbf{b}(t) = \mathbf{s}(t) * \mathbf{a}(t) \quad (3)$$

where $\mathbf{s}(t)$ is a time-domain scattering matrix describing the system, $\mathbf{a}(t)$ and $\mathbf{b}(t)$ are the forward and backward time-domain traveling wave vectors, respectively, and $*$ is used to denote convolution.

The package interconnect subsystem can be represented as an S-parameter block as shown in Fig. 6. Here, S_{pkg} is the scattering parameter matrix of the multiport subsystem representing the package. The connection scattering matrix, equation (4), of the network shown in Fig. 6, relates the incident and reflected waves at all network ports with the excitation of the network [10].

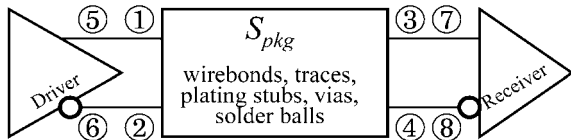


Fig. 6. An S-parameter block representation of a PBGA package system.

Based on the network topology, the connection scattering matrix of the system in Fig. 6 is given as

$$\begin{bmatrix} S_{55} & 0 & -1 & 0 & 0 & 0 & 0 \\ 0 & S_{66} & 0 & -1 & 0 & 0 & 0 \\ -1 & 0 & S_{11} & S_{12} & S_{13} & S_{14} & 0 & 0 \\ 0 & -1 & S_{21} & S_{22} & S_{23} & S_{24} & 0 & 0 \\ 0 & 0 & S_{31} & S_{32} & S_{33} & S_{34} & 0 & -1 \\ 0 & 0 & S_{41} & S_{42} & S_{43} & S_{44} & -1 & 0 \\ 0 & 0 & 0 & 0 & 0 & -1 & S_{77} & 0 \\ 0 & 0 & 0 & 0 & -1 & 0 & 0 & S_{88} \end{bmatrix} \times \begin{bmatrix} a_5 \\ a_6 \\ a_1 \\ a_2 \\ a_3 \\ a_4 \\ a_7 \\ a_8 \end{bmatrix} = \begin{bmatrix} E \\ -E \\ 0 \\ 0 \\ 0 \\ 0 \\ 0 \\ 0 \end{bmatrix} \quad (4)$$

The scattering parameters are denoted by S_{ij} , and the vector a_i 's are the incident waves at all ports and the right-hand side vector is the vector of independent signal generators, E , in the system. For given excitations, the impulse responses of the S-parameter blocks are convolved to solve the whole system.

A more complex system, such as the memory interconnect system shown in Fig. 7(a) can be represented as a cascade of S-parameter blocks as shown in Fig. 7(b). In order to handle the nonlinear driver and receiver networks, each S-parameter block is treated as a multiterminal device in the *MNA* matrix of the global circuit equation. The forward and the backward traveling waves are expressed in terms of node voltages and branch currents using

$$\begin{bmatrix} a_i \\ b_i \end{bmatrix} = \begin{bmatrix} \frac{V_i + Z_i I_i}{2\sqrt{R_i}} \\ \frac{V_i - Z_i^* I_i}{2\sqrt{R_i}} \end{bmatrix} \quad (5)$$

where Z_i is the reference impedance, $R_i = Re(Z_i)$, and V_i and I_i are terminal voltages and currents, respectively. The stamp of the *MNA* matrix for direct integration of the scattering matrix corresponding to

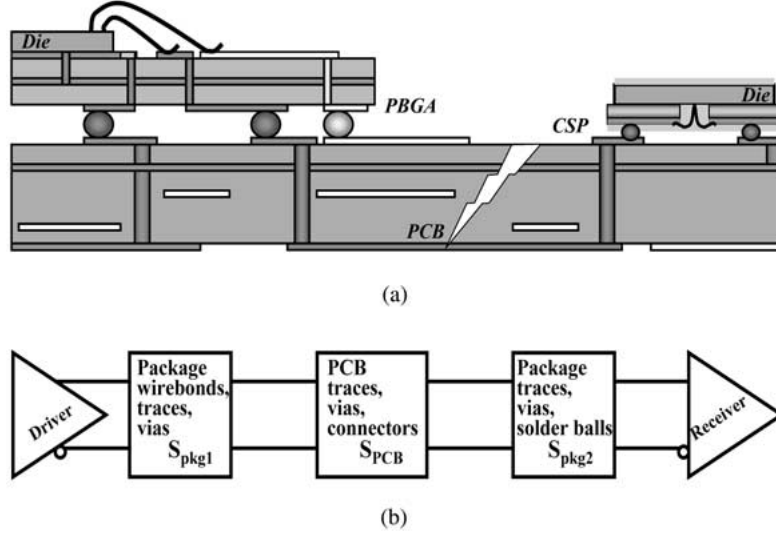


Fig. 7. A memory channel interconnect system. (a) A board-level interconnect system, (b) A cascade of S-parameter blocks.

the S-parameter block is

$$\begin{bmatrix} I - S_{11} & -(I - S_{11}) & -S_{12}\sqrt{\frac{R_1}{R_2}} & S_{12}\sqrt{\frac{R_1}{R_2}} & -(S_{11}Z_1 + Z_1^*) & -S_{12}Z_2\sqrt{\frac{R_1}{R_2}} \\ -S_{21}\sqrt{\frac{R_2}{R_1}} & S_{21}\sqrt{\frac{R_2}{R_1}} & I - S_{22} & -(I - S_{22}) & -S_{21}Z_1\sqrt{\frac{R_2}{R_1}} & -(S_{22}Z_2 + Z_2^*) \end{bmatrix} \begin{bmatrix} I \\ -I \\ I \\ -I \\ V_1^+ \\ V_1^- \\ V_2^+ \\ V_2^- \\ I_1 \\ I_2 \end{bmatrix} = \begin{bmatrix} 0 \\ 0 \end{bmatrix} \quad (6)$$

where Z_i and I are the $n \times n$ reference impedance and the identity submatrices, respectively. The real part of the reference impedance is defined as, $R_i = |\text{Re}(Z_i)|$. The pairs (V_1, V_2) and (I_1, I_2) are terminal voltages and currents, respectively. Then, the transient analysis of the interconnect system is performed by using *IFFT* to calculate the time-domain waveforms of the entries in (6) and apply the discrete time solution to solve the whole system, including the nonlinear devices, for given input waveforms.

IV. Simulation Results

To demonstrate the simulation methodology based on S-parameter using the proposed windows and convolution technique, the Tukey window is implemented in

Agilent Advanced Design System (ADS) simulation tool using the ADS Application Engineering Language (AEL) [11]. The ADS linear equation-based model is used to incorporate the windowed scattering parameters into the interconnect network. Then the ADS convolution engine is used to perform the time-domain simulation.

First, the method is applied to analyze several versions of the wirebond package design shown in Figs. 8 and 9. As shown in Fig. 8, the top and bottom layers of the design are wiring layers. There are two power planes in the middle. The dielectric coefficient of the material is $\epsilon_r = 3.9$. There are four pairs of nets with wirebonds and solder balls at the input and output ports, respectively. The inner and outer pairs have short and long plating stubs, respectively. The scattering parameters of a 16-port network are obtained using

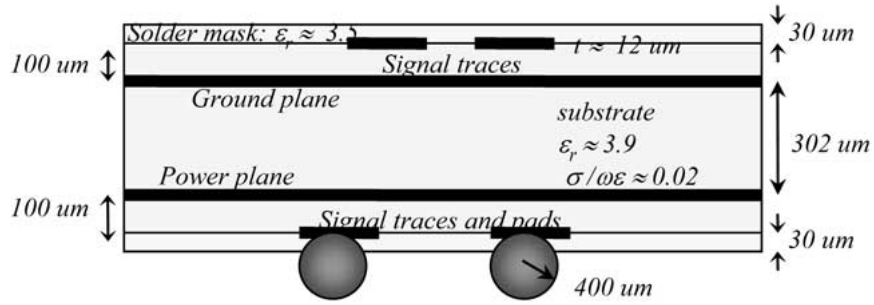


Fig. 8. The cross section of the PBGA package.

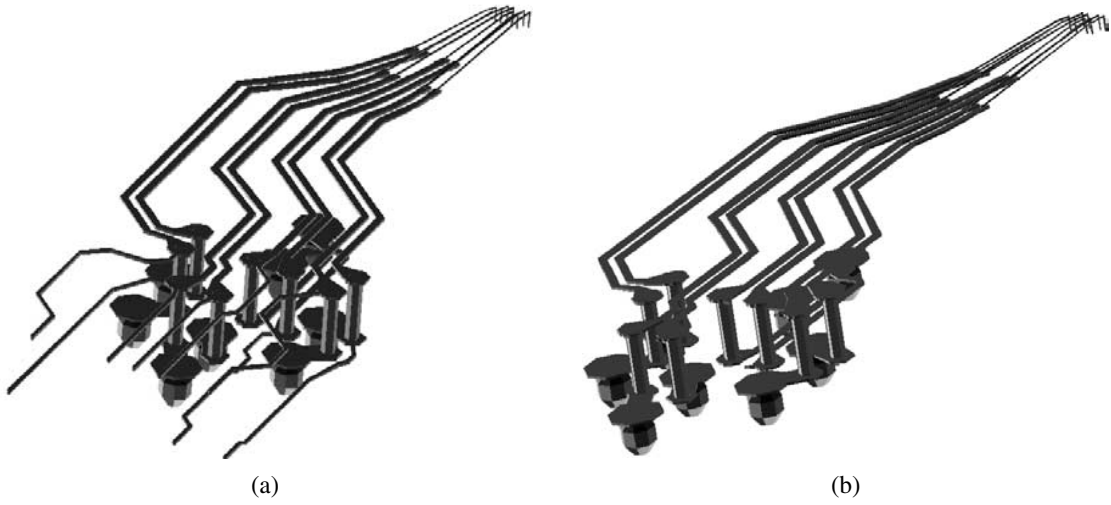


Fig. 9. The PBGA package nets. (a) Four pairs of nets with plating stubs, (b) Four pairs of nets without plating stubs.

a fullwave electromagnetic solver. The scattering parameters of the package without the plating stub are obtained similarly. The transfer coefficients with and without the plating stubs, S_{21} , of the inner and outer pairs are shown in Fig. 10. The transfer curves of the nets with plating stubs show first resonance at 8.6 GHz and 14.7 GHz, as shown in Figs. 10(a) and 10(b), respectively. These first resonance frequencies correlate well to the quarter wavelength of the length of the plating stubs given by,

$$f_o = \frac{1}{4l} \frac{c_o}{\sqrt{\epsilon_r}} \quad (7)$$

where c_o is the speed of light, ϵ_r is the relative permittivity or dielectric constant of the substrate, and l is the length of the plating stub. The 4.4 mm and 2.6 mm long plating stubs show the first lowest and highest resonance frequencies, respectively.

To perform convolution, the scattering parameters are first bandlimited using Tukey windows. The magnitude of the original and the band-limited scattering parameters are shown in Fig. 11(a). Since the loss in the package is small and the interconnects are short, the transmission coefficients, S_{21} , do not approach zero at high frequencies. For a lossy system, however, bandlimiting may not be required, since S_{21} is naturally bandlimited. On the other hand, the reflection and coupling coefficients approach nonzero constants as the frequency increases. Thus, bandlimiting of such coefficients is always essential to avoid aliasing when performing the *IFFT*. The bandlimited scattering parameters closely approximate the original up to higher and higher frequencies as the Tukey parameters approach 1 as shown in Fig. 11(a). However, as the frequency range over which the original and bandlimited S_{21} match increases, the time-domain waveform, $s_{21}(t)$

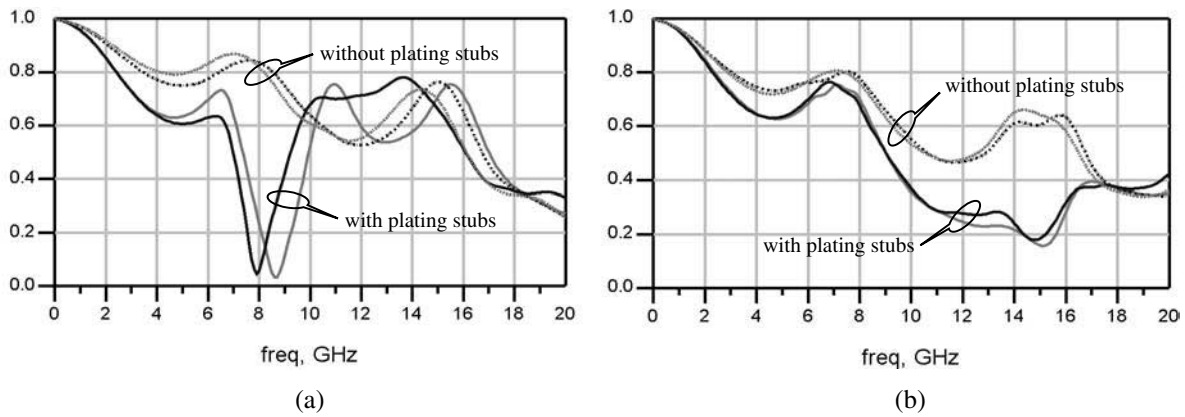


Fig. 10. The magnitude of the transfer coefficients, S_{21} , of the true (dark lines) and the complement (gray lines) nets for the PBGA package. (a) PBGA outer pairs. Nets with 4.5 mm long stubs (solid lines), (b) PBGA inner pairs. Nets with 2.6 mm long stubs (solid lines).

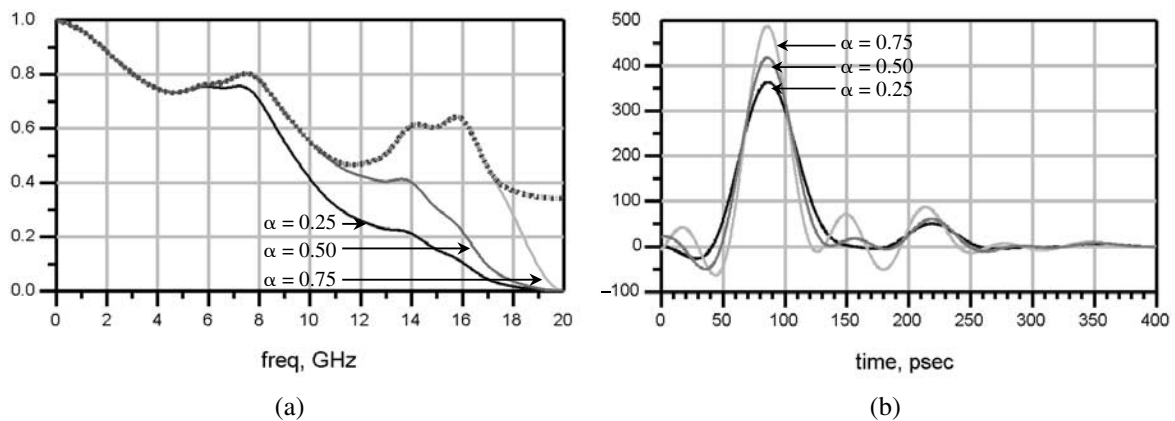


Fig. 11. The bandlimited signals for $\alpha = 0.25$, (dark line), $\alpha = 0.50$, (gray line), $\alpha = 0.75$, (light gray line), tapered Tukey windows. (a) Frequency-domain transfer coefficients, $S_{21}(\omega)$. (b) Time-domain responses, $s_{21}(t)$.

shows more ripples as shown in Fig. 11(b). The choice of the window parameter, α , depends on the rise time of the signal. Therefore, in order to accurately determine the voltage and timing margins, the proper selection and application of a window and window constants are critical.

In Fig. 12, a Tukey filter with window constant $\alpha = 0.5$ is applied to calculate the voltage and timing budgets for the PBGA with and without the plating stubs. The PBGA package with plating stub shows larger reflections, about 23 mV more, on the transmitted waveforms at the wirebonds, as shown in Fig. 12(a). The received waveforms at the solder balls of the package with plating stubs show smaller amplitude

and a longer delay, about 10 ps more, as shown in Fig. 12(b).

The second example is the system of a PCB board and connector interconnect system, shown in Fig. 13, through which the PBGA package communicates with another package. The four-port scattering parameters of the PCB and connector system are measured in the frequency range of 50 MHz–20 GHz using an Agilent 8722ES vector network analyzer (VNA) [12]. The input reflection coefficient, S_{11} , of each net approaches unity as the frequency increases. The measured and bandlimited reflection coefficient of one of the nets is shown in Fig. 14. Several well-known windows considerably modify the measured data after 3.5 GHz.

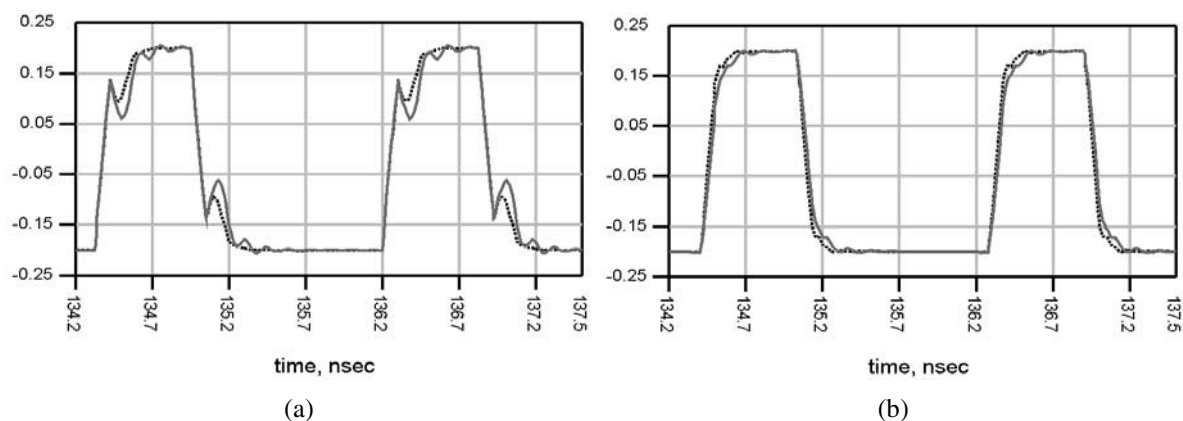


Fig. 12. The responses of the PBGA package with (gray line) and without (dark line) plating stubs. (a) Waveforms at the input, (b) Waveforms at the output.

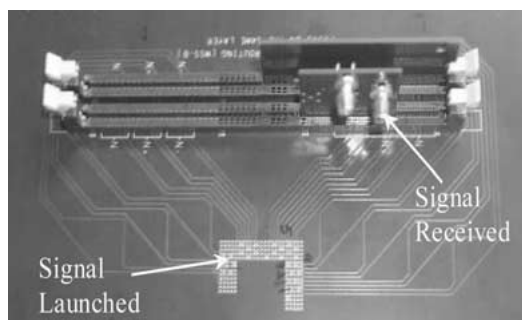


Fig. 13. The PCB and connector prototype.

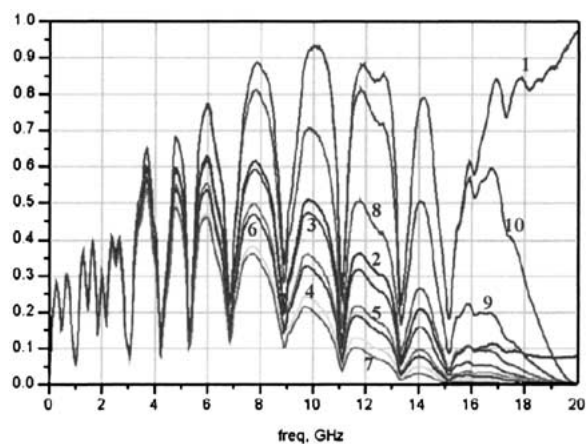


Fig. 14. The bandlimiting effects of some of the classic windows on $S_{11}(\omega)$. The windows are: 1: Rectangular; 2: Hamming; 3: Hanning; 4: Gaussian; 5: Kaiser-Bessel; 6: Blackman; 7: Blackman-Harris; 8: Tukey ($\alpha = 0.25$); 9: Tukey ($\alpha = 0.50$); 10: Tukey ($\alpha = 0.75$).

This severely limits the useful frequency range of the modified scattering parameters. However, the Tukey windows considerably extend the useful frequency range and consequently lessen the requirement to measure the parameters over a much wider frequency range.

For the complete time-domain simulation, the measured scattering parameters are band-limited using a Tukey window with window constant, $\alpha = 0.25$. The transmission coefficient, S_{21} is naturally bandlimited. Thus, the difference between the measured and approximated values of S_{21} over the frequency range is small, as shown in Figs. 15(a) and 15(b). Using the bandlimited scattering parameters, a simulation of the PCB and connector system is performed using the 3.2 Gb/s, 32-bit input waveform, shown in Fig. 16(a), obtained from a measurement using a data generator [13]. The transmitted waveforms of the PCB and connector system are shown in Fig. 16(b). The system shows sufficient voltage and timing margins for reliable operation at 3.2 Gb/s. The simulated and measured output eye diagrams are shown in Fig. 17(a) and 17(b), respectively. The correlation between the measured and simulated waveforms is excellent.

Finally, to compare the efficiencies of the convolution-based and circuit-based methods, the three test cases listed in Table 2 are considered. The three test cases have different degrees of complexity in terms of geometry, delay, loss, reflection, and coupling. The first test case is a package via structure. This 3D structure has a small loss, delay, and reflection. First, the two-port scattering parameters of the structure are obtained from full-wave electromagnetic solver. Next, the

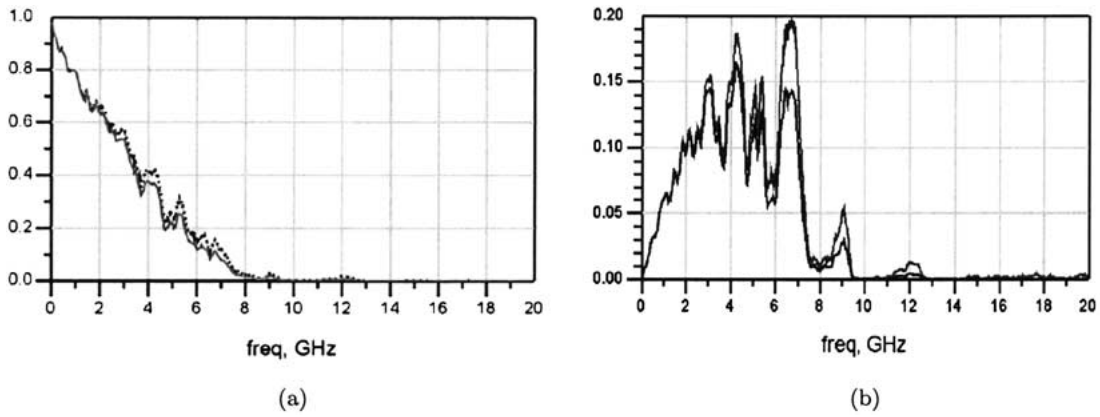


Fig. 15. Measured (dark dashed line) and bandlimited (gray solid line) scattering parameters of the PCB and connector system. (a) Magnitude of transfer coefficient, $|S_{21}|$, (b) Magnitude of far-end coupling coefficient, $|S_{41}|$.

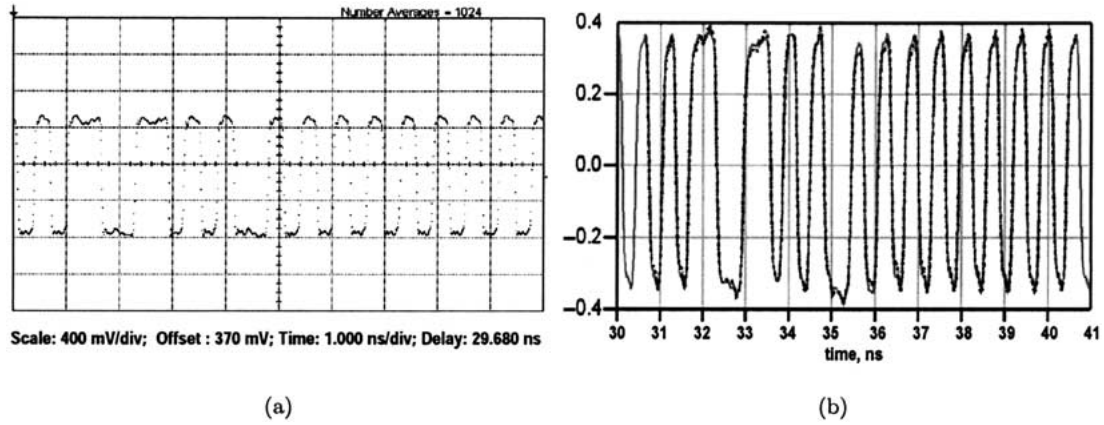


Fig. 16. The time-domain measured (dark dashed line) and simulated (gray solid line) responses of the PCB and connector system. (a) A 32-bit input waveform obtained from measurement, (b) Measured and simulated output waveforms.

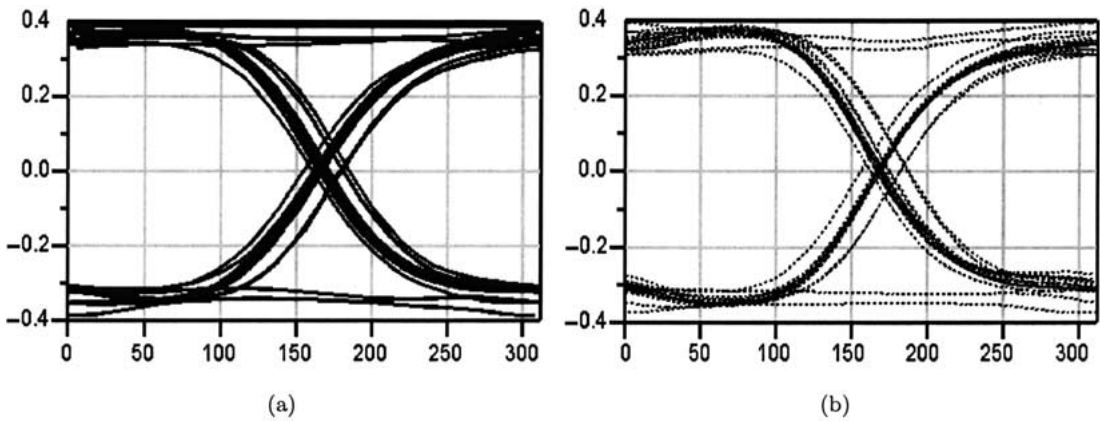


Fig. 17. Measured and simulated eye diagrams of the PCB and connector system using the measured 32-bit pattern of Fig. 16(a). (a) Simulated output response, (b) Measured output response.

Table 2. Comparisons of the circuit-based and convolution-based simulation methods.

Test Cases	Delay	Reflection	Loss	Coupling	# Circuit Elements	Circuit-based CPU Time	Convolution CPU Time
A package via	Very small	Some	Small	None	136	10 sec.	1.6 sec.
Coupled microstrips	Large (1 ns)	Small	Small	Large	1500	287 min.	2.1 sec.
A memory channel	Large (2 ns)	Large	Large	Large	1400	184 min.	5.0 sec.

S parameters are approximated by a network of 136 circuit elements to include the structure in a conventional circuit-based simulator.

The second test case is a coupled microstrip system. These 6-in. long uniform microstrips are mainly 2D structures with significant delay, but low loss and reflection. First, the four-port scattering parameters of this system are obtained from VNA measurements. Next, the S parameters are approximated using a network with over 1500 circuit elements.

The third test case is a memory channel. This channel has significant loss, delay, reflection, and coupling. First, the four-port scattering parameters are calculated from frequency-domain simulation. Next, the S parameters are approximated by a network consisting of over 1400 circuit elements.

The simulations are performed by terminating the test cases at the source and load with resistors and applying voltage sources with 3.2 Gbps bit pattern. The simulations of all test cases are carried out up to 100 ns. They are included in convolution- and circuit-based simulators as S parameter blocks and networks, respectively. The simulation times for the test cases using the conventional circuit-based and convolution-based methods are shown in Table 2. Even though the simulation CPU time for the circuit-based approach does not include the time for extracting the circuit parameters from the frequency-domain scattering parameters, the convolution-based method is faster by order of magnitude than the circuit-based method.

Against conventional belief, the convolution-based method is faster for simulating interconnect systems. In the circuit-based approach, the system (MNA) matrices that need to be solved at each time point are large due to the large number of circuit elements needed to accurately approximate the frequency-domain parameters. Often these approximating networks include small inductors and capacitors that decrease the convergence rates and consequently the efficiency of the simulation algorithms.

V. Conclusions

In this paper, we have presented a methodology to perform accurate transient analysis of package interconnect systems using convolution. The windowing technique is introduced to improve the accuracy of the convolution method by reducing undesired effects associated with the transformation of the frequency-domain parameters. The bandlimiting improves the accuracy of the results by generating finite-duration impulse responses, and dampening the unwanted ringing, as well as avoiding aliasing errors. The effects of the bandlimiting filters is studied in detail. Some of the classic windows are also compared.

Using the frequency-domain parameters directly in simulation minimizes the error introduced when converting the scattering parameters to more familiar network parameters to develop circuit representations. Thus, the method avoids trial and error and optimization to extract model parameters. Through the use of the proposed method, it is possible to very accurately calculate the timing and voltage margins of a memory system. This enables the study of the frequency-dependent behavior of the interconnects and the effects of the plating stubs, wirebonds, vias, and solderballs at high frequencies on the overall performance of the package. The examples show that such an accurate analysis is critical as the data rates increase to several gigabits per second and the signal voltage swings lower to a few hundred millivolts. An excellent correlation is obtained between the measurement and simulated results of a PCB and connector system.

References

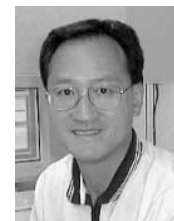
1. Glaskowsky, P. N., "Rambus rolls out Yellowstone." *Microprocessor Report*, July 15, 2002.
2. Beyene, W., Yuan, C., Cheng, N. and Wu, H., "Interconnect design and modeling of a 3.2 Gb/s/pair bi-directional memory

- system.” *DesignCon 2002: High Performance System Design Conference*. Santa Clara, CA, January 28–31, 2002.
3. Oh, K. S., “Accurate transient simulation of transmission lines with the skin effects.” *IEEE Transactions on Computer-Aided of Integrated Circuits and Systems* 19(3), pp. 389–396, March 2000.
 4. Coelho, C. P., Philips, J. R. and Silveria, L. M., “Robust rational function approximation algorithm for model generation,” in *Proceedings of the 36th Design Automation Conference*, New Orleans, LA, June 1999.
 5. Djordjevic, A., Sarkar, T. and Harrington, R., “Analysis of lossy transmission lines with arbitrary nonlinear terminations.” *IEEE Transactions on Microwave Theory and Techniques* 33(6), pp. 660–665, June 1986.
 6. Schutt-Ainé, J. and Mittra, R., “Scattering parameter transient analysis of transmission lines loaded with nonlinear terminations.” *IEEE Transactions on Microwave Theory and Techniques* 36(3), pp. 529–536, March 1988.
 7. Winklestein, D., Steer, M. B. and Pomerleau, R., “Simulation of arbitrary transmission line networks with nonlinear terminations.” *IEEE Transactions on Circuits and Systems* 38(4), pp. 418–422, April 1991.
 8. Harris, F. J., “On the use of window for harmonic analysis with the Discrete Fourier Transform,” in *Proceedings of IEEE* 66, pp. 51–83, January 1978.
 9. Nuttall, A. H., “Some windows with good sidelobe behavior.” *IEEE Transactions on Acoustics, Speech, and Signal Processing* ASSP-29(1), pp. 84–91, February 1981.
 10. Dobrowolski, J. A. and Ostrowski, W., *Computer-Aided Analysis, Modeling and Design of Microwave Networks: The Wave Approach*. Boston: Artech House, Inc., 1996.
 11. *Agilent Advanced Design System Users Guide*. Agilent Technologies, Santa Rosa, CA, 2001.
 12. *Agilent 8722ES Network Analyzer Operating and Programming Manual*. Agilent Technologies, Santa Rosa, CA, February 2001.
 13. *Agilent 8133A 3 GHz Pulse Generator Users Guide*. Agilent Technologies, Santa Rosa, CA, February 2000.



Wendemagegnehu (Wendem) T. Beyene was born in Addis Ababa, Ethiopia. He received his B.S. and

M.S. degrees in electrical engineering from Columbia University, in 1988 and 1991 respectively, and his Ph.D. degree in electrical and computer engineering from University of Illinois at Urbana-Champaign, in 1997. From 1988 to 1994, he was with the IBM, Microelectronics division, Fishkill, NY, where he designed and analyzed advanced multilayer packages. From 1997 to 2000, he was with Hewlett-Packard Company and Agilent Technologies EEs of EDA at Westlake Village, CA working on analog and RF circuit simulation tools. In 2000, he joined Rambus Inc., Los Altos, CA as a signal integrity engineer. Presently, he is involved in modeling and analyses of chip-to-chip interconnect systems and measurements of voltage and timing margins of high-speed memory systems. His professional interests include efficient circuit simulation techniques, advanced signaling techniques, and I/O circuitry. Dr. Beyene is a member of Eta Kappa Nu, Tau Beta Pi, IEEE, and SIAM.



Xingchao Chuck Yuan was born in Jiangsu, China. He received his B.S. degree in electrical engineering from Southeast University, Nanjing, China, in 1982, and his M.S. and Ph.D. degrees in electrical engineering from Syracuse University, Syracuse, New York in 1983 and 1987, respectively. Under the guidance of Prof. Roger F. Harrington, his doctoral research was on modeling high frequency electromagnetic coupling into apertures using Method of Moments. From 1987 to 1990, he was a post doctoral fellow and later a research assistant professor at Dartmouth College, where he conducted research in microwave hyperthermia treatment planning. He was among the first to develop hybrid methods combining Method of Moments with finite element method for modeling complex problems such as a human body. From 1990 to 1995, he was with Ansoft Corporation, Pittsburgh, Pennsylvania, where he was in charge of developing *HFSS*, now an industrial standard for modeling complex 3D structures at

RF/microwave frequencies. He developed new computational techniques that sped up *HFSS* from 10X to 100X so that it became a practical modeling and analysis tool. From 1995 to 1998, he was with Cadence Design Systems, in Chelmsford, Massachusetts, where he was involved in developing design and modeling signal integrity/EMI tools for high speed printed circuit boards and packages. In 1998 he joined with Rambus

Inc., Los Altos, California, where he is a signal integrity manager responsible for designing, modeling, and implementing Rambus high speed signaling technologies. He has a number of publications in technical journals and conferences. His professional interests include computational electromagnetic methods and high speed signaling technologies for multi-gigabit applications.